Comparative phosphoproteome profiling reveals a function of the STN8 kinase in fine-tuning of cyclic electron flow (CEF)

Sonja Reiland[a,b], Giovanni Finazzi[c,d,e,f], Anne Endler[a,b], Adrian Willig[g,h], Katja Baerenfaller[a,b], Jonas Grossmann[a,b], Bertran Gerrits[a,b], Dorothea Rutishauser[a,b], Wilhelm Gruissem[a,b], Jean-David Rochaix[g,h], and Sacha Baginsky[a,b,1,2]

[a]Department of Biology, Eidgenössische Technische Hochschule (ETH) Zurich, 8092 Zurich, Switzerland; [b]Functional Genomics Center Zurich, 8057 Zurich, Switzerland; [c]Centre National Recherche Scientifique, Unité Mixte Recherche 5168, Laboratoire Physiologie Cellulaire et Végétale, F-38054 Grenoble, France; [d]Commissariat à l'Energie Atomique et Energies Alternatives, l'Institut de Recherches en Technologies et Sciences pour le Vivant, F-38054 Grenoble, France; [e]Université Grenoble 1, F-38041, France; [f]Institut National Recherche Agronomique, UMR1200, F-38054 Grenoble, France; and Departments of [g]Molecular Biology and [h]Plant Biology, University of Geneva, 1211 Geneva, Switzerland

Edited* by Bob B. Buchanan, University of California, Berkeley, CA, and approved June 24, 2011 (received for review March 24, 2011)

Important aspects of photosynthetic electron transport efficiency in chloroplasts are controlled by protein phosphorylation. Two thylakoid-associated kinases, STN7 and STN8, have distinct roles in short- and long-term photosynthetic acclimation to changes in light quality and quantity. Although some substrates of STN7 and STN8 are known, the complexity of this regulatory kinase system implies that currently unknown substrates connect photosynthetic performance with the regulation of metabolic and regulatory functions. We performed an unbiased phosphoproteome-wide screen with *Arabidopsis* WT and *stn8* mutant plants to identify unique STN8 targets. The phosphorylation status of STN7 was not affected in *stn8*, indicating that kinases other than STN8 phosphorylate STN7 under standard growth conditions. Among several putative STN8 substrates, PGRL1-A is of particular importance because of its possible role in the modulation of cyclic electron transfer. The STN8 phosphorylation site on PGRL1-A is absent in both monocotyledonous plants and algae. In dicots, spectroscopic measurements with *Arabidopsis* WT, *stn7*, *stn8,* and *stn7*/*stn8* double-mutant plants indicate a STN8-mediated slowing down of the transition from cyclic to linear electron flow at the onset of illumination. This finding suggests a possible link between protein phosphorylation by STN8 and fine-tuning of cyclic electron flow during this critical step of photosynthesis, when the carbon assimilation is not commensurate to the electron flow capacity of the chloroplast.

phosphoproteomics | *Arabidopsis thaliana*

In the field of chloroplast biogenesis, interest in protein phosphorylation historically focused on photosynthesis-related proteins, with the initial discovery of thylakoid membrane protein phosphorylation dating back to the late 1970s (1–4). Almost a decade later, AtpB, RNA-binding proteins, and transcription factors were recognized as phosphoproteins in thylakoid membranes and stroma fractions (5–7). Because of recent large-scale functional genomics and phosphoproteomics approaches, ~200 chloroplast phosphoproteins are known today, and several kinases have been identified that are most likely involved in their phosphorylation (8). However, the exact kinase/substrate relationships are not known for most of the proteins, and efforts are underway to identify in vivo substrates of known kinases. Phosphoproteomics data suggest that chloroplast functions are regulated by a highly complex phosphoprotein network in which one kinase phosphorylates several substrates and one substrate is probably phosphorylated by several kinases at different sites (9, 10).

Although we currently do not understand all nodes in the chloroplast phosphoprotein network, candidate proteins and experimental tools are available to address the above questions. Two of the best-characterized chloroplast kinases are STN7 and STN8. STN7 is the ortholog of the Stt7 kinase from *Chlamydomonas reinhardtii* that was identified in screens for strains with a defect in state transitions (11). This process balances the absorbed light excitation energy between the two photosystems. State transitions are regulated by light quality and intensity and mediated by phosphorylation of photosystem II (PSII) light-harvesting complex (LHCII) proteins (4, 12). It is now well established that STN7 activity is required for state transitions, although it is currently unclear whether STN7 directly phosphorylates LHCII proteins or triggers their phosphorylation through a cascade. STN8 is a paralog of STN7 and is also associated with the thylakoid membrane system. Analyses with phosphothreonine-specific antibodies identified the D1 (PsbA) and D2 (PsbD) proteins of PSII, PsbH, CP43, and a Ca^{2+}-sensitive thylakoid phosphoprotein, calcium-sensing receptor (CaS), as STN8 substrates (13–15). However, loss of STN8 function not only affects the phosphorylation of thylakoid membrane proteins but also the expression of nucleus- and plastid-encoded genes for photosynthetic proteins (13).

These data suggest multiple functional interactions of STN8 within the chloroplast phosphoprotein network that extend beyond our current mechanistic knowledge. For example, light-quality–dependent changes of photosystem core protein phosphorylation mediated by STN8 no longer occur in the *stn7* background in *Arabidopsis*, suggesting functional crosstalk between STN7 and STN8 (16, 17). The *Chlamydomonas* ortholog of STN8, called Stl1, is a phosphoprotein in vivo whose phosphorylation depends on Stt7 (18). It is conceivable that a similar crosstalk exists between the corresponding *Arabidopsis* orthologs STN8 and STN7. However, although STN7 is an abundant phosphoprotein, comprehensive phosphoproteome analyses failed to identify any STN8 phosphorylation in *Arabidopsis* chloroplasts under different conditions (9, 10, 19). Interestingly, the sequence of the C-terminal region of STN7 containing the four mapped phosphorylated sites diverges from the corresponding region in Stt7, suggesting a function of STN7 phosphorylation in adaptation processes that are specific to higher plants (10). Although it is

Author contributions: S.R., G.F., J.-D.R., and S.B. designed research; S.R., G.F., A.E., and A.W. performed research; S.R., G.F., K.B., J.G., B.G., D.R., W.G., J.-D.R., and S.B. analyzed data; and G.F. and S.B. wrote the paper.

The authors declare no conflict of interest.

*This Direct Submission article had a prearranged editor.

Data deposition: The MS data and tandem MS spectra have been deposited in the PRoteomics IDEntifications (PRIDE) database, http://www.ebi.ac.uk/pride/ (accession nos. 13754–13761).

[1]Present address: Institute of Biochemistry and Biotechnology, Martin-Luther-University Halle-Wittenberg, 06120 Halle (Saale), Germany.

[2]To whom correspondence should be addressed. E-mail: sacha.baginsky@biochemtech.uni-halle.de.

This article contains supporting information online at www.pnas.org/lookup/suppl/doi:10.1073/pnas.1104734108/-/DCSupplemental.

currently unknown which kinase phosphorylates STN7, analysis of the phosphorylation motifs has suggested that one of the phosphorylation sites might be used by casein kinase II (10).

Here we report STN8 substrates that we identified in a comparative proteome-wide analysis of protein phosphorylation in WT and in STN8-deficient (*stn8*) plants. We quantified unphosphorylated proteins in plastids of both genotypes by normalized spectral counting to distinguish changes in phosphorylation states from changes in protein abundance. Our data show that other kinase(s) besides STN8 are involved in the phosphorylation of STN7 and establish PGRL1-A as a STN8 substrate.

Results and Discussion

Phosphoproteome Profiling from *stn8* and WT *Arabidopsis* Leaf Tissue. We analyzed the leaf phosphoproteome of WT and *stn8* plants in three biological replicates by using a combined immobilized metal-ion affinity chromatography/titanium dioxide affinity chromatography (IMAC/TiO_2) phosphopeptide enrichment strategy followed by LTQ-Orbitrap mass spectrometry (MS). In total, 15,492 spectra were assigned to 3,589 phosphopeptides and 1,738 unique phosphoproteins at a false-discovery rate of 0.15% at the spectrum level. All information concerning peptide and protein identifications are deposited in the PRoteomics IDEntifications (PRIDE) database (20). To extract plastid phosphoproteins, we matched this dataset against a chloroplast proteome reference table that was assembled from the overlap of two previously published chloroplast proteome datasets (*SI Appendix*, Table S1) (10, 21). Altogether, 1,657 spectra, 294 phosphopeptides, and 149 phosphoproteins matched with chloroplast proteins (*SI Appendix*, Table S2). Chloroplast phosphopeptide detection was similar to previously reported analyses, and 131 of the phosphoproteins of *stn8* and WT were previously identified (9, 10, 19), whereas 18 unknown proteins were detected in our analysis. The reproducible detection of these chloroplast phosphoproteins suggests that we have acquired a robust dataset that reflects phosphorylation activity in chloroplasts under standard conditions. All identified phosphoproteins and peptides are provided in *SI Appendix*, Table S2.

A global qualitative comparison of phosphoprotein identification and phosphorylation motif utilization in WT and *stn8* chloroplasts revealed minor differences at the level of phosphopeptide detection (*SI Appendix*, Fig. S1). We therefore searched for quantitative differences in the phosphorylation state of chloroplast proteins by using the workflow presented in Fig. 1.

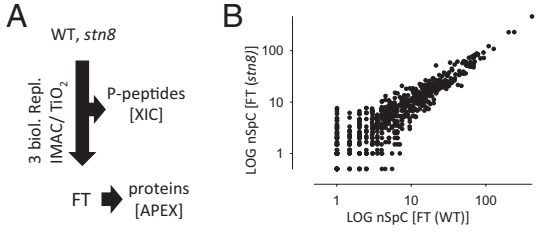

Fig. 1. Strategy for the quantification of phosphopeptides and unphosphorylated proteins. (*A*) WT or *stn8* samples were subjected to affinity chromatography on IMAC or TiO_2 as described in *Materials and Methods*. Phosphopeptides were eluted from the affinity column and identified by MS. The relative quantification of phosphopeptides in the different samples was based on their spectral count information and extracted ion chromatograms (XIC). The unphosphorylated peptides were collected in the flow-through fraction and were used for the quantification of chloroplast proteins by normalized spectral counting (nSpC) in two biological replicates. Absolute protein expression (APEX). (*B*) Comparison of the abundance of chloroplast proteins in the flow-through fractions from WT and *stn8* samples. The diagram shows the averaged normalized spectral count information from the IMAC flow-through, plotted on a logarithmic scale.

Quantitative phosphopeptide analysis was performed in three biological replicates by spectral counting and extracted ion chromatogram quantification (Fig. 1*A*). To distinguish between changes in protein abundance and changes in phosphorylation state, we quantified the unphosphorylated proteins from the flow-through fraction of the IMAC. The protein quantification from the flow-through enables a quantitative comparison of the plastid proteomes in the two different genetic backgrounds (Fig. 1*B* and *SI Appendix*, Table S3). The average Spearman rank correlation coefficient, ρ, for the spectral count data from 756 identified chloroplast proteins is 0.871, suggesting minor quantitative adaptations of the chloroplast proteome to a loss of STN8 (Fig. 1*B*). The high similarity between the plastid proteomes of WT and *stn8* plants allowed a valid quantitative comparison of protein phosphorylation in the plastids of the two genotypes.

Quantitative Comparison of Phosphopeptide Detection in WT and STN8-Deficient Plants. We searched for phosphoproteome differences between WT and *stn8* plants by comparing the spectral count information for individual phosphopeptides in WT and *stn8* datasets, which we considered to be different when they were detected with at least three spectra in total and a twofold higher spectral count in WT in at least two biological replicates. We furthermore included relative phosphopeptide quantification by comparing extracted ion chromatograms using the Progenesis software tool (Nonlinear Dynamics). We used both criteria, i.e., reduced spectral count and reduced relative intensities of extracted ion chromatograms in *stn8*, together to assess the effect of loss of STN8 function. This stringent combination of selection criteria provides a reliable assessment of those peptides whose phosphorylation is affected in *stn8*.

We first asked whether STN7 phosphorylation was affected in *stn8* plastids. None of the STN7 phosphopeptides fulfilled the criteria for differentially phosphorylated peptides described above, suggesting that STN8 is not required to maintain the STN7 phosphorylation state. The extracted ion chromatogram quantification confirms that STN7 phosphopeptides are phosphorylated to a similar extent in both genotypes (Table 1 and Fig. 2). The peptide NALApSALR, with the phosphorylation site at serine, was even increased in abundance in *stn8* in all three replicates (Table 1 and Fig. 2, which shows the third replicate). The reversed-phase chromatography separated two isobaric phosphopeptides that were phosphorylated at different threonine residues (Fig. 2 *Center*). Although the peptide eluting at 45 min was identified as TVTEpTIDEISDGRK by manual spectrum annotation, the peptide that eluted at 51 min was pTVTETIDEISDGRK, TVpTETIDEISDGRK, or a mixture of both (*SI Appendix*, Fig. S2). The fragmentation pattern does not allow us to distinguish between these two possibilities. The two isobaric peptides have the same abundance in WT and *stn8* plants, and the same holds true for the doubly phosphorylated peptide pp [TVTETIDEISDGRK] in all three replicates (Table 1 and Fig. 2). Together, our data strongly suggest that STN8 is not responsible for STN7 phosphorylation under our experimental conditions.

Differential Quantitative Phosphopeptide Detection in WT and *stn8* Plants. The previously reported STN8 substrates CaS (At5G23060) (15), the doubly phosphorylated PsbH peptide ApTQpTVEDSSR (Table 1) (14), as well as RbcL (ATCG00490), two unknown proteins (AT1G54520 and AT5g08540), the thylakoid-associated proteins CP29 (AT3G08940), and an ATP synthase family protein (AT4G32260) (Table 1) were identified with higher spectral counts in WT compared with *stn8* and fulfill the criteria for differential phosphorylation. The two unknown proteins contain one and two transmembrane domains, respectively, and both were previously identified in the proteome of chloroplast membrane preparations (22–24). Although the thylakoid association of a majority of the above proteins makes their phosphorylation by

Table 1. Protein and phosphopeptide detection and quantification in WT and STN8-deficient plants

Protein			Spectral count replicates						Log abundance ratio (WT/*stn8*)			Log ratio protein expression[a] (WT/*stn8*)
Identifier	Annotation	Phosphopeptide	WT (1)	WT (2)	WT (3)	Stn8 (1)	Stn8 (2)	Stn8 (3)	Exp. 1	Exp. 2	Exp. 3	
Reported substrates												
ATCG00710	PsbH	pp[ATQTVEDSSR(SGPR)]	10	12	12	8	2	5	−0.2/only WT[b]	5.2	4.6	−0.2
		p[ATQTVEDSSR(SGPR)]	18	19	14	22	30	9	−2.3	−0.3	−3.3	
		p[Ac-ATQTVEDSSR(SGPR)]	4	0	1	1	2	0	−1.0	−1.7	1.3	
		pp[Ac-ATQTVEDSSR(SGPR)]	2	0	1	0	0	0	ND	9.4	ND	
ATCG00020	PsbA	p[Ac-TAILERR]	—	—	—	—	—	—	−3.3	ND	1.9	−0.1
		p[TAILERR]	—	—	—	—	—	—	−0.2	ND	ND	
ATCG00270	PsbD	p[TIALGKFTK]	—	—	—	—	—	—	2.1	ND	ND	0.1
		p[Ac-TIALGKFTK]	3	0	0	2	0	0	0.8	ND	2.8	
ATCG00280	CP43	p[Ac-TLFNGTLALAGR]	—	—	—	—	—	—	−1.7	0.6	−1.0	−0.1
		p[TLFNGTLALAGR]	—	—	—	—	—	—	Only WT	3.4	−0.7	
		pp[Ac-TLFNGTLALAGR]	—	—	—	—	—	—	ND	ND	−1.7	
AT5G23060	CaS	p[SGTKFLPSSD]	2	2	1	2	0	0	0.8	2.7	2.8	0.2
		p[IIPAASRSFGTR]	0	0	1	0	0	1	0.3	ND	ND	
		pp[IIPAASRSFGTR]	—	—	—	—	—	—	−0.7	ND	ND	
		p[LGTDSYNFSFAQVLSPSR]	2	1	0	1	1	0	−0.5	1.5	ND	
		p[SFGTRSGTK]	1	0	0	1	0	0	−1.3	ND	ND	
Substrates in question												
AT1G68830	STN7	p[TVTETIDEISDGRK]	9	2	7	5	2	8	0.8	ND	−0.2	0.1
		pp[TVTETIDEISDGRK]	12	1	5	9	2	5	0.1	0.9	−1.0	
		p[NALASALR]	1	0	2	2	2	4	−1.7	−1.0	−1.0	
New substrates												
AT4G04020	Fibrillin	p[ATDIDDEWGQDGVER]	2	0	2	0	0	0	2.0	ND	1.1	0.4
ATCG00490	RbcL	p[WSPELAAACEVWK]	0	1	2	0	0	1	ND	ND	ND	−0.1
At1G54520	Unknown	p[SSSSSSSQSYSVPR]	1	0	2	0	0	1	−0.3	ND	−0.3	1.6
At5G08540	Unknown	p[KNSSVEEETEEEVEEDMPWIQEK]	3	0	1	1	0	0	0.2	ND	ND	0.7
AT3G08940	LHCB4.2	p[NLYGEVIGTRTEAVDPK]	3	3	0	2	1	0	0.8	1.2	−0.2	−0.1
AT4G32260	ATP synthase	p[ALDSQIAALSEDIVKK]	1	1	2	0	0	0	Only WT	−0.4	0.5	0.2
AT1G08640	Unknown	p[GVTFGSFK]	7	1	1	1	0	0	2.1	ND	2.4	0.6
AT4G22890	PGRL1	p[ATTEQSGPVGGDNVDSNVLPYCSINK]	2	3	2	0	0	1	2.2	6.0	0.7	0.8

Acetylated phosphopeptides were assigned by Progenesis on the basis of MASCOT search results (*Materials and Methods*). Listed are the identified phosphopeptides, their number of spectra in the individual replicates, and the abundance ratio of the precursor extracted ion chromatogram as calculated by Progenesis. The quantification was done without considering phosphopeptides with oxidized methionine and did not distinguish the site of phosphorylation in a peptide with several hydroxylated amino acids. We furthermore quantified all identified chloroplast proteins in the flow-through fractions from the phosphopeptide affinity chromatography by normalized spectral counting. ND, not detected; p, phosphorylation; Ac, acetylation.

[a]Ratio of the mean normalized spectral count quantities expressed as Log base 2.

[b]Only detected in WT in the strong cation exchange chromatography fraction 3 from the membrane preparation.

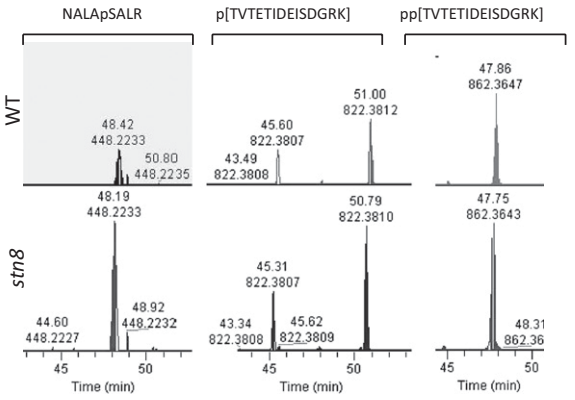

Fig. 2. Phosphopeptide quantification of phosphorylation sites in STN7. Displayed is the intensity (*y* axis) over time during chromatography (retention time, *x* axis) for the mass window [calculated phosphopeptide mass ± 5 ppm]. (*Upper*) Phosphopeptide intensity in WT. (*Lower*) Phosphopeptide intensity in the *stn8* mutant. The intensity of the precursor with higher intensity was set to 100%, and the same *y* axis scale was used for the other precursor to allow a direct comparison. Presented are representative data for the STN7 phosphopeptides from the third replicate.

STN8 possible, the extracted ion chromatogram quantification does not support the conclusion that their phosphorylation is reduced in *stn8* (Table 1). Although this finding does not exclude that the two proteins are STN8 targets, our data suggest that their phosphorylation is largely independent of STN8 under the experimental conditions and is likely catalyzed by at least one other chloroplast protein kinase.

Nevertheless, three proteins showed consistently reduced phosphorylation in *stn8* based on spectral count and extracted ion chromatogram quantification. One of these is fibrillin (AT4G04020), which is phosphorylated at the threonine residue in ATDIDDEWGQDGVER, which represents the most N-terminal tryptic peptide detectable in vivo (25). Fibrillin is associated with plastoglobuli and located on the stromal side of thylakoid membranes, a topology that supports phosphorylation by STN8. The second protein is annotated as "unknown protein" (AT1G08640). This protein was previously identified in chloroplast proteome analyses as an envelope protein with three transmembrane domains, and it is thought to be a solute transporter of cyanobacterial endosymbiotic origin (26). The phosphorylation site in the peptide GVTFGSFKVSK is located at the N-terminal side of the three predicted transmembrane domains. Although the consistent trend in spectral count and extracted ion chromatogram quantifications is to argue for the dependence of this phosphorylation site on STN8, it is currently unclear how the phosphorylation of an envelope membrane protein is catalyzed by a thylakoid-associated kinase. It is possible that transient interactions between thylakoid and chloroplast envelope membranes could allow for such an STN8-mediated phosphorylation. Alternatively, STN8 could be part of a phosphorylation cascade that results in the phosphorylation of AT1G08640.

The third protein with a reduced phosphorylation state in *stn8* is the PGR5-like protein PGRL1-A (AT4G22890), which was characterized further (*SI Appendix*, Figs. S3–S5). PGRL1-A is a thylakoid membrane protein with two transmembrane domains and its N-terminal end exposed to the stromal side (27). This protein is most likely phosphorylated at one of the two threonine residues in ATTEQSGPVGGDNVDSNVLPYCSINK (*SI Appendix*, Figs. S3 and S4). According to the predicted transit peptide cleavage site at position 60 (28) and in vivo large-scale proteome mapping (25), this phosphopeptide represents the most N-terminal tryptic peptide of the mature protein. PGRL1-A forms a protein complex with PGR5 that is associated with (but not bound to) photosystem I (PSI). Plants that lack PGRL1-A show perturbations in their cyclic electron flow (CEF) response, which appears as an accelerated transition from CEF to linear electron flow (LEF) during the dark-to-light transition, i.e., the activation of photosynthesis (27). We therefore investigated possible changes of CEF in *stn8*, which would support a functional role for PGRL1-A phosphorylation during this phase. To identify a potential effect of loss of PGRL1-A phosphorylation and to determine its specificity for *stn8*, we measured parameters related to LEF and CEF in *stn8*, *stn7*, and *stn7*/*stn8* double mutants.

Transition from CEF to LEF Is Altered in Plants Deficient in the STN8 Kinase. In steady-state photosynthesis, LEF involves both PSII and PSI activity, producing ATP and NADPH and finally leading to CO_2 assimilation. Conversely, a significant fraction of the photo-generated electrons can be recycled around PSI (CEF) at the onset of illumination, i.e., when the Calvin cycle is still largely inactive while the electron flow capacity is already at maximum (29). The transition from CEF to LEF was first assayed by measuring the kinetics of P_{700} oxidation upon illumination with far-red light, i.e., under conditions where PSI is preferentially excited. In dark-adapted conditions, slow P_{700} oxidation rates are observed, whereas P_{700} oxidation is accelerated upon light exposure for 10 min (*SI Appendix*, Fig. S6), in agreement with previous findings (27, 30). This period corresponds to the time required to activate carbon assimilation (31). Starting with dark-adapted leaves, similar kinetics was seen in all of the genotypes when activity was probed at the beginning of illumination (30 s; *SI Appendix*, Fig. S6), suggesting a similar CEF capacity. Similarly, no differences were measured at the end of illumination (10 min), indicating the same rate of LEF, consistent with previous data (11, 13). In contrast, a faster transition from slow to fast P_{700} oxidation was seen in *stn8* and the *stn7*/*stn8* double mutant compared with WT or *stn7* (*SI Appendix*, Fig. S6 and Fig. 3), suggesting a faster transition from CEF to LEF in the absence of STN8. To confirm this conclusion, PSII activity was estimated from fluorescence parameters (32) (*SI Appendix*, Fig. S7*A*) and compared with the overall rate of electron flow [from the electrochromic shift (ECS); *SI Appendix*, Fig. S7*B* and Table S4] to

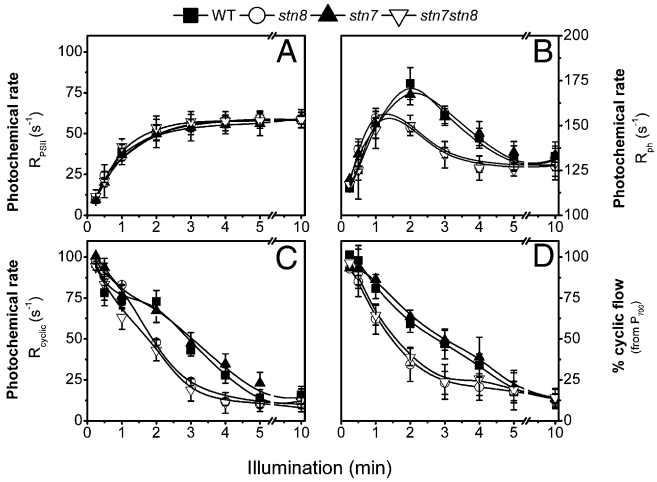

Fig. 3. Transition from CEF to LEF during a dark-to-light shift is faster in *stn8* and *stn7*/*stn8* than in WT. Dark-adapted leaves from WT, *stn7*, *stn8*, and the *stn7*/*stn8* double mutant were exposed to red light (37 $\mu E \cdot m^{-2} \cdot s^{-1}$). At any indicated time, PSII activity (*A*), the sum of PSII plus PSI activity (*B*), the rate of CEF (*C*), and the fraction of PSI involved in CEF (*D*) were measured. Data refer to the average of six samples from two independent experiments (± SE). Parameters were derived from fluorescence, P_{700}, and ECS measurements as detailed in *SI Appendix*, *SI Materials and Methods*.

derive changes in the rate of CEF. The ECS is a light-induced shift in the absorption spectrum of some photosynthetic pigments, which is caused by charge separation within the two photosystems (33). During illumination, PSII activity increased in the same way in all genotypes (Fig. 3*A*), and the PSI + PSII electron flow rate was higher in the STN8-containing lines (Fig. 3*B*). Although the estimated rate of cyclic PSI activity (Fig. 3*C*) (34) was similar in dark- and light-adapted leaves, a faster deactivation was observed in *stn8* and *stn7*/*stn8* compared with the WT and *stn7*, in agreement with the P_{700}-derived data (Fig. 3*D*), suggesting that the loss of PGRL1 phosphorylation does not impair CEF or LEF activity but does impact the plant's capacity to maintain an active CEF during the onset of carbon assimilation. This phenotype is very similar to the one observed in *pgr5* (35) and *pgrl1* (27), two mutants lacking a protein complex (PGR5/PGRL1) likely involved in the regulation of CEF. In both mutants, maximum CEF capacity is unchanged relative to WT when tested under the same conditions as here (27, 30), but a faster activation of LEF occurs upon light exposure. This similarity between *pgr5*, *pgrl1*, and *stn8* and *stn7*/*stn8* supports our proposal for a link between PGRL1-A phosphorylation and CEF stability.

Conclusion

The large-scale analysis reported here demonstrates that phosphoproteome profiling is a powerful tool for kinase characterization and for the detection of unique and unexpected kinase targets. Because our identification of unknown STN8 substrates was based on stringent selection criteria, we identified a restricted set of STN8 targets, and our analysis most likely underestimates their number. Among them, PGRL1-A is particularly interesting because it suggests a link between protein phosphorylation and modulation of electron flow in plants. This possibility is supported by the modified CEF capacity observed in *stn8* and the *stn7*/*stn8* double mutant (which both lack STN8 activity) in the experimental conditions reported above. Because the observed effect on CEF is transitory, it could be relevant under rapidly changing light conditions, such as shading by light flecks, which is consistent with a fast-operating control mechanism such as phosphorylation. However, the faster deactivation of CEF observed in plants lacking STN8 has no apparent effect on the overall rate of carbon assimilation, which is similar in WT, *stn8*, *stn7*, and the double mutant (Fig. 3*A*). This finding rules out the possibility of a direct effect of STN8 on the carbon assimilatory process, at least under the conditions explored in this work. Recently, a protein supercomplex has been identified in *Chlamydomonas* that is capable of performing CEF and contains stoichiometric amounts of PSI, the cytochrome b_6f complex (including the small subunit PetO), ferredoxin:NADPH oxidoreductase (FNR), LHCI, LHCII, and PGRL1 (36). Its accumulation in thylakoids is related to the activation of the Stt7 kinase during state transitions. The complex does not contain PGR5, and it was proposed that this protein would be replaced in *Chlamydomonas* by PetO, which also undergoes phosphorylation under state 2 conditions (37). Based on these findings, it is therefore tempting to speculate that modulation of CEF by protein phosphorylation could be a possible leitmotif in electron flow regulation in Viridiplantae. In *Chlamydomonas*, this process would operate through sequestering of diffusing carriers within the PetO-driven cyclic supercomplex. In plants, where PetO is absent and no CEF supercomplex has been found so far (31), the STN8/PGRL1-A system could directly or indirectly control the transition between CEF and LEF in a freely diffusing system through a still-unknown mechanism. Alternatively, phosphorylation of PGRL1 could stabilize a supercomplex involved in CEF, similar to the one found in *Chlamydomonas* (36). Consistent with the specificity of the STN8/PGRL1-A regulatory pathway, a comparison of the PGRL1-A sequences in different photosynthetic organisms reveals that the phosphorylation site identified in *Arabidopsis* is absent in mosses, green algae, and other marine photosynthetic organisms (*SI Appendix*, Fig. S8). Intriguingly, this site is also absent in monocots, suggesting that the N-terminal STN8-mediated phosphorylation of PGRL1-A originated after the separation of dicots from monocots. At present, the exact mechanism how PGRL1-A phosphorylation modulates the transition kinetics between CEF and LEF remains to be explored.

Materials and Methods

Plant Material, Growth Conditions, and Protein Extraction. *Arabidopsis thaliana* Col0 and *stn8* (SALK 060869) seedlings were grown on soil under short-day conditions in a controlled environment chamber (8 h light/16 h dark, 100 $\mu E \cdot m^{-2} \cdot s^{-1}$). Plants were harvested after 6 wk, 3 h after the start of the light, and immediately frozen in liquid nitrogen, ground, and subsequently stored at −80 °C until further analyses. Proteins were extracted exactly as described previously (10) (*SI Appendix, SI Materials and Methods*).

In-Solution Tryptic Protein Digest. Before tryptic digestion, cysteine residues were reduced with 10 mM DTT for 45 min at 50 °C and alkylated by 50 mM iodoacetamide for 1 h at room temperature in the dark. Trypsin (sequencing grade; Promega) was added in a ratio of 1:20 and incubated over night at 37 °C.

Fractionation of Peptides by Strong Cation Exchange Chromatography. Peptides were desalted by using Sep-Pak reverse-phase cartridges (Waters), dissolved in buffer A [10 mM KH_2PO_4 (pH 2.6) in 25% acetonitrile] and loaded onto a 4.6 × 200 mm PolySULFOETHYL Aspartamide A column (PolyLC) on an Agilent HP1100 binary HPLC system. Peptides were eluted with an increasing KCl gradient [10-40 min at 0–30% buffer B then 40–60 min at 30–100% buffer B; buffer B: 10 mM KH_2PO_4 (pH 2.6) and 350 mM KCl in 25% acetonitrile]. The eluate was fractionated into four fractions and desalted with Sep-Pak reverse-phase cartridges (Waters).

IMAC. Chelating Sepharose Fast Flow beads (GE Healthcare) were charged four times with 0.1 M $FeCl_3$ freshly prepared solution and washed four times with washing buffer (74:25:1 water:acetonitrile:acetic acid). Desalted peptides were acidified with 0.1% TFA in 25% acetonitrile, applied to 40 μL of 25% bead slurry, and incubated for 30 min at room temperature. Samples were washed five times with washing buffer and once with water. Phosphopeptides were eluted by adding 30 μL of 100 mM sodium phosphate buffer (pH 8.9). The pH of all samples was adjusted to 3 by adding drops of 10% TFA followed by desalting and concentrating samples with ZipTips (μC18; Millipore).

TiO_2 Affinity Chromatography. Phosphopeptides were enriched using TiO_2 affinity chromatography as described by Bodenmiller et al. (38) with minor modifications. Peptides were desalted and dissolved in phthalic acid solution (80% acetonitrile, 2.5% TFA, and 0.13 M phthalic acid). The peptide mixture was incubated with 0.3 mg of TiO_2 (GL Science) for 30 min in closed Mobicol spin columns. After different washing steps (*SI Appendix, SI Materials and Methods*), peptides were eluted with 0.3 M NH_4OH and dried in a speed vac. Before MS analysis, samples were desalted with ZipTips (μC18; Millipore).

Analysis by Liquid Chromatography/Electrospray Ionization/Tandem MS and Interpretation of MS Data. Phosphopeptide analysis was performed with an LTQ-Orbitrap as described previously (10) (*SI Appendix, SI Materials and Methods*). Up to five data-dependent tandem MS spectra were acquired in the linear ion trap for each Fourier transform MS spectral acquisition range, the latter acquired at 60,000 FWHM nominal resolution settings with an overall cycle time of ~1 s. The samples were acquired by using internal lock mass calibration on *m/z* 429.088735 and 445.120025. Tandem MS spectra were searched with Mascot (Matrix Science) version 2.2.04 against The *Arabidopsis* Information Resource (TAIR9) protein database (downloaded on June 29, 2009) with concatenated decoy database supplemented with contaminants (67,079 entries) as described previously (10) (*SI Appendix, SI Materials and Methods*) and integrated into the pep2pro database (39). Identifications with a MASCOT ion score >30 and a MASCOT expected value of <0.015 were accepted. Phosphorylation site assignment was based on normalized delta ion score (ΔI) that was calculated for phosphopeptides for which the only difference between the rank 1 and the rank 2 hit was the phosphorylation position. Phosphorylation site assignments with $\Delta I \geq 0.4$ were accepted (10, 40). From the final data, PRIDE 2.1 XML files were created and exported to the PRIDE database (20) (accession nos. 13754–13761). Data are also available in the pep2pro database (www.pep2pro.ethz.ch) (39). Relative quantification by extracted ion chromatograms was achieved by commercial Progenesis software from Nonlinear Dynamics. Analysis was performed in pairs of liquid chromatography/MS runs for WT and the corresponding *stn8* experiment, according to the manufacturer's instructions. The quantitative analysis was done in three biological replicates.

Spectroscopic Analysis. Spectroscopic changes were followed on intact leaves with a flash spectrophotometer (JTS 10; Biologic). P_{700} oxidation kinetics was assessed at 820–870 nm, and fluorescence was probed in the near infrared upon excitation with blue light. The ECS was measured at 520–545 nm to avoid interference by redox-related signals (*SI Appendix, SI Materials and Methods*). Actinic light was provided by a red LED peaking at 620 nm, which was transiently switched off to allow for the measurements of the P_{700} and ECS changes (*SI Appendix, SI Materials and Methods*).

ACKNOWLEDGMENTS. We are grateful for support from the Functional Genomics Center Zurich, especially for the advice of Drs. Bernd Roschitzki and Peter Gehrig concerning the interpretation of MS data. This work was supported by funds from ETH Zurich and Swiss SystemsX.ch Project Plant Growth Regulation (to W.G.), by CNRS funds (to G.F.), and by Swiss National Foundation Grant 31003A_133089 (to J.-D.R.). S.R. was supported by Marie Curie Early Stage Training Fellowship ADONIS MEST-CT-2005-020232 (to W. G. and S.B.). A.E. was supported by a Zurich-Basel Plant Science Center Graduate Research Fellowship (to S.B.).

1. Allen JF, Bennett J, Steinback KE, Arntzen CJ (1981) Chloroplast protein-phosphorylation couples plastoquinone redox state to distribution of excitation-energy between photosystems. *Nature* 291:25–29.
2. Bennett J (1977) Phosphorylation of chloroplast membrane polypeptides. *Nature* 269: 344–346.
3. Lemeille S, Rochaix JD (2010) State transitions at the crossroad of thylakoid signalling pathways. *Photosynth Res* 106:33–46.
4. Rochaix JD (2007) Role of thylakoid protein kinases in photosynthetic acclimation. *FEBS Lett* 581:2768–2775.
5. Kanekatsu M, Munakata H, Furuzono K, Ohtsuki K (1993) Biochemical characterization of a 34 kDa ribonucleoprotein (p34) purified from the spinach chloroplast fraction as an effective phosphate acceptor for casein kinase II. *FEBS Lett* 335:176–180.
6. Kanekatsu M, Saito H, Motohashi K, Hisabori T (1998) The β subunit of chloroplast ATP synthase (CF_0CF_1-ATPase) is phosphorylated by casein kinase II. *Biochem Mol Biol Int* 46:99–105.
7. Baginsky S, Tiller K, Link G (1997) Transcription factor phosphorylation by a protein kinase associated with chloroplast RNA polymerase from mustard (*Sinapis alba*). *Plant Mol Biol* 34:181–189.
8. Baginsky S, Gruissem W (2009) The chloroplast kinase network: New insights from large-scale phosphoproteome profiling. *Mol Plant* 2:1141–1153.
9. Lohrig K, Müller B, Davydova J, Leister D, Wolters DA (2009) Phosphorylation site mapping of soluble proteins: Bioinformatical filtering reveals potential plastidic phosphoproteins in *Arabidopsis thaliana*. *Planta* 229:1123–1134.
10. Reiland S, et al. (2009) Large-scale *Arabidopsis* phosphoproteome profiling reveals novel chloroplast kinase substrates and phosphorylation networks. *Plant Physiol* 150: 889–903.
11. Bellafiore S, Barneche F, Peltier G, Rochaix JD (2005) State transitions and light adaptation require chloroplast thylakoid protein kinase STN7. *Nature* 433:892–895.
12. Murata N (2009) The discovery of state transitions in photosynthesis 40 years ago. *Photosynth Res* 99:155–160.
13. Bonardi V, et al. (2005) Photosystem II core phosphorylation and photosynthetic acclimation require two different protein kinases. *Nature* 437:1179–1182.
14. Vainonen JP, Hansson M, Vener AV (2005) STN8 protein kinase in *Arabidopsis thaliana* is specific in phosphorylation of photosystem II core proteins. *J Biol Chem* 280: 33679–33686.
15. Vainonen JP, et al. (2008) Light regulation of CaS, a novel phosphoprotein in the thylakoid membrane of *Arabidopsis thaliana*. *FEBS J* 275:1767–1777.
16. Bräutigam K, et al. (2009) Dynamic plastid redox signals integrate gene expression and metabolism to induce distinct metabolic states in photosynthetic acclimation in *Arabidopsis*. *Plant Cell* 21:2715–2732.
17. Dietzel L, Pfannschmidt T (2008) Photosynthetic acclimation to light gradients in plant stands comes out of shade. *Plant Signal Behav* 3:1116–1118.
18. Lemeille S, Turkina MV, Vener AV, Rochaix JD (2010) Stt7-dependent phosphorylation during state transitions in the green alga *Chlamydomonas reinhardtii*. *Mol Cell Proteomics* 9:1281–1295.
19. Sugiyama N, et al. (2008) Large-scale phosphorylation mapping reveals the extent of tyrosine phosphorylation in *Arabidopsis*. *Mol Syst Biol* 4:193.
20. Vizcaíno JA, et al. (2010) The Proteomics Identifications database: 2010 update. *Nucleic Acids Res* 38(Database issue):D736–D742.
21. Yu QB, et al. (2008) Construction of a chloroplast protein interaction network and functional mining of photosynthetic proteins in *Arabidopsis thaliana*. *Cell Res* 18: 1007–1019.
22. Sun Q, et al. (2009) PPDB, the Plant Proteomics Database at Cornell. *Nucleic Acids Res* 37(Database issue):D969–D974.
23. Kleffmann T, Hirsch-Hoffmann M, Gruissem W, Baginsky S (2006) plprot: A comprehensive proteome database for different plastid types. *Plant Cell Physiol* 47:432–436.
24. Ferro M, et al. (2010) AT_CHLORO, a comprehensive chloroplast proteome database with subplastidial localization and curated information on envelope proteins. *Mol Cell Proteomics* 9:1063–1084.
25. Baerenfaller K, et al. (2008) Genome-scale proteomics reveals *Arabidopsis thaliana* gene models and proteome dynamics. *Science* 320:938–941.
26. Tyra HM, Linka M, Weber AP, Bhattacharya D (2007) Host origin of plastid solute transporters in the first photosynthetic eukaryotes. *Genome Biol* 8:R212.
27. DalCorso G, et al. (2008) A complex containing PGRL1 and PGR5 is involved in the switch between linear and cyclic electron flow in *Arabidopsis*. *Cell* 132:273–285.
28. Emanuelsson O, Brunak S, von Heijne G, Nielsen H (2007) Locating proteins in the cell using TargetP, SignalP and related tools. *Nat Protoc* 2:953–971.
29. Johnson GN (2005) Cyclic electron transport in C3 plants: Fact or artefact? *J Exp Bot* 56:407–416.
30. Nandha B, Finazzi G, Joliot P, Hald S, Johnson GN (2007) The role of PGR5 in the redox poising of photosynthetic electron transport. *Biochim Biophys Acta* 1767:1252–1259.
31. Breyton C, Nandha B, Johnson GN, Joliot P, Finazzi G (2006) Redox modulation of cyclic electron flow around photosystem I in C3 plants. *Biochemistry* 45:13465–13475.
32. Genty B, Harbinson J, Briantais J-M, Baker NR (1990) The relationship between non-photochemical quenching of chlorophyll fluorescence and the rate of photosystem 2 photochemistry in leaves. *Photosynth Res* 25:249–257.
33. Witt HT (1979) Energy conversion in the functional membrane of photosynthesis. Analysis by light pulse and electric pulse methods. The central role of the electric field. *Biochim Biophys Acta* 505:355–427.
34. Joliot P, Joliot A (2002) Cyclic electron transfer in plant leaf. *Proc Natl Acad Sci USA* 99: 10209–10214.
35. Munekage Y, et al. (2002) PGR5 is involved in cyclic electron flow around photosystem I and is essential for photoprotection in *Arabidopsis*. *Cell* 110:361–371.
36. Iwai M, et al. (2010) Isolation of the elusive supercomplex that drives cyclic electron flow in photosynthesis. *Nature* 464:1210–1213.
37. Hamel P, Olive J, Pierre Y, Wollman FA, de Vitry C (2000) A new subunit of cytochrome b_6f complex undergoes reversible phosphorylation upon state transition. *J Biol Chem* 275:17072–17079.
38. Bodenmiller B, Mueller LN, Mueller M, Domon B, Aebersold R (2007) Reproducible isolation of distinct, overlapping segments of the phosphoproteome. *Nat Methods* 4: 231–237.
39. Baerenfaller K, et al. (2011) pep2pro: a new tool for comprehensive proteome data analysis to reveal information about organ-specific proteomes in Arabidopsis thaliana. *Integr Biol* (*Camb*) 3:225–237.
40. Beausoleil SA, Villén J, Gerber SA, Rush J, Gygi SP (2006) A probability-based approach for high-throughput protein phosphorylation analysis and site localization. *Nat Biotechnol* 24:1285–1292.